**Atmospheric
Chemistry
and Physics
Discussions**

Equatorial wave
analysis from SABER
and ECMWF
temperatures

M. Ern et al.

Title Page	
Abstract	Introduction
Conclusions	References
Tables	Figures
◄◄	►►
◄	►
Back	Close
Full Screen / Esc	

Printer-friendly Version

Interactive Discussion

EGU

Equatorial wave analysis from SABER and ECMWF temperatures

M. Ern[1], P. Preusse[1], M. Krebsbach[1,*], M. G. Mlynczak[2], and J. M. Russell III[3]

[1]Institute for Stratospheric Research (ICG-1), Forschungszentrum Juelich, Juelich, Germany
[2]Atmospheric Sciences Division, NASA Langley Research Center, Hampton, VA, USA
[3]Center for Atmospheric Sciences, Hampton University, Hampton, VA, USA
[*]now at: Department of Physics, University of Wuppertal, Wuppertal, Germany

Correspondence to: M. Ern (m.ern@fz-juelich.de)

M. Ern et al.

Full Screen / Esc

EGU

Abstract

Equatorial planetary scale wave modes such as Kelvin waves or Rossby-gravity waves are excited by convective processes in the troposphere. In this paper an analysis for these and other equatorial wave modes is carried out with special focus on the stratosphere using temperature data from the SABER instrument as well as ECMWF temperatures. Space-time spectra of symmetric and antisymmetric spectral power are derived to separate the different equatorial wave types and the contribution of gravity waves is determined from the spectral background of the space-time spectra.

Both gravity waves and equatorial planetary scale wave modes are main drivers of the quasi-biennial oscillation (QBO) in the stratosphere. Temperature variances attributed to the different wave types are calculated for the period from February 2002 until March 2006 and compared to previous findings. A comparison between SABER and ECMWF wave analyses shows that in the lower stratosphere SABER and ECMWF spectra and temperature variances agree remarkably well while in the upper stratosphere ECMWF tends to overestimate Kelvin wave components. Gravity wave variances are partly reproduced by ECMWF but have a significant low-bias. A case study for the time period of the SCOUT-O3 tropical aircraft measurement campaign in Darwin/Australia (in November and December 2005) is performed and we find that in the lower stratosphere also the longitude-time distribution of the Kelvin waves is correctly reproduced by ECMWF.

1 Introduction

Equatorial wave modes, such as, for example, Kelvin waves or Rossby-gravity waves, are forced in the tropical troposphere by convective processes (e.g., Pires et al., 1997; Straub and Kiladis, 2003; Lindzen, 2003; Randel and Wu, 2005). Together with a broad spectrum of gravity waves they are the main drivers of the quasi-biennial oscillation (QBO) in the stratosphere (Hitchman and Leovy, 1988; Dunkerton, 1997; Baldwin et

al., 2001). As a result of the interaction with the QBO winds tropical wave activity itself shows modulations due to the QBO.

The QBO is relevant for the stability of the subtropical mixing barrier of the so-called "tropical pipe", which is more stable during QBO easterly phases. Therefore equatorial
5 waves play an indirect but important role for the modulation of mixing processes between the troposphere and the stratosphere by meridional transports (Shuckburgh et al., 2001). Also many other processes in atmospheric chemistry and dynamics in the stratosphere and mesosphere (even at high latitudes) are modulated or influenced by the QBO, showing the importance of the driving equatorial wave modes (Baldwin et al.,
10 2001). Another important effect directly connected with tropical wave activity is tropical upwelling: Wave drag, tropical and subtropical, is an important mechanism for driving the observed annual mean tropical upwelling in the lower stratosphere (Semeniuk and Shepherd, 2001).

A theoretical description of planetary scale equatorial wave modes was first given by
15 Matsuno (1966) who derived the properties of the different wave types from solutions of the shallow-water model on an equatorial beta plane with the Coriolis parameter:

$$f = \beta y \tag{1}$$

where y is the meridional distance from the equator and β is the gradient of the Coriolis parameter at the equator. This leads to the following dispersion relation:

$$20 \quad \frac{\sqrt{gh_e}}{\beta} \left(\frac{\hat{\omega}^2}{gh_e} - k^2 - \frac{k\beta}{\hat{\omega}} \right) = 2n + 1, \quad n = 0, 1, 2, \ldots \tag{2}$$

with $\hat{\omega}$ the intrinsic frequency of the wave, k the zonal wavenumber, g the gravity acceleration, n the order of the solution, and h_e the so-called equivalent depth. The wave modes described by Eq. 2 are trapped near the equator because the Coriolis parameter f changes its sign at the equator.
25 The equivalent depth is connected with the vertical wavenumber m as given in Eq. 3

Equatorial wave analysis from SABER and ECMWF temperatures

M. Ern et al.

Title Page

Abstract	Introduction
Conclusions	References
Tables	Figures

|◄ | ►|

◄ | ►

Back | Close

Full Screen / Esc

Printer-friendly Version

Interactive Discussion

EGU

(e.g., Wu et al., 2000; Lindzen, 2003).:

$$m^2 = \left(\frac{N^2}{gh_e} - \frac{1}{4H^2} \right) \qquad (3)$$

with N the buoyancy frequency, and H the pressure scale height.

Equatorial waves can be divided into eastward and westward traveling waves, as well as into wave modes symmetric and antisymmetric with respect to the equator.

In the following the most important wave modes are introduced. For atmospheric temperature the most prominent eastward traveling symmetric wave modes are Kelvin waves (e.g., Tindall et al., 2006a) and, with much smaller amplitude, eastward traveling inertia-gravity waves with $n=1$. Eastward traveling antisymmetric modes are inertia-gravity waves with $n=0$ and $n=2$. Westward traveling symmetric modes are equatorial Rossby waves with $n=1$ and inertia-gravity waves with $n=1$, whereas westward traveling antisymmetric wave modes are equatorial Rossby waves and inertia-gravity waves, both with $n=2$, and Rossby-gravity waves.

Figure 1 shows the spectral ranges between the lines for equivalent depths of $h_e=8$ and 90 m in the horizontal wavenumber/frequency domain. These spectral bands are typical for the abovementioned wave modes in the troposphere (Wheeler and Kiladis, 1999) and in the following we will call these wave bands "tropospheric" wave bands. Equivalent depths of 8 and 90 m correspond to vertical wavelengths between about 2.8 and 9.4 km in the stratosphere and due to the lower buoyancy frequency N to about 5.6 and 19 km in the troposphere (see Eq. 3). The tropospheric values can be attributed to the vertical scale of convective processes which act as sources of the waves. It is usually assumed that half the vertical wavelength observed corresponds to the depth of the convective systems acting as source (e.g., Chang, 1976; Fulton and Schubert, 1985; Salby and Garcia, 1987). This behavior is similar for gravity waves excited by convection (Alexander et al., 1995). The abovementioned range of tropospheric vertical wavelengths is in good agreement with the vertical profiles of thermal forcing in convective systems which have a broad maximum over about 2–8 km in the middle

troposphere (e.g., Chang, 1976; Fulton and Schubert, 1985; Johnson and Ciesielski, 2000).

The phenomenon of Kelvin waves in the oceans is well known for a long time. In the stratosphere first evidence for Kelvin waves was found by Wallace and Kousky (1968) and Rossby-gravity waves were first detected by Yanai and Maruyama (1966) (therefore Rossby-gravity waves sometimes are called Yanai-waves).

Since then numerous studies about equatorial waves have been carried out based on radiosonde data, e.g., Angell et al. (1973); Sato et al. (1994), as well as satellite data providing a global view of the atmosphere. Some examples using stratospheric satellite data are, e.g., Salby et al. (1984); Randel et al. (1990); Randel and Gille (1991); Bergman and Salby (1994); Canziani et al. (1994); Srikanth and Ortland (1998); Tsai et al. (2004); Randel and Wu (2005); Ratnam et al. (2006).

However, all these studies had one or several of the following shortcomings: the data used had only poor spatial or temporal resolution, limited altitude coverage, or the data sets were too short. One of the consequences is that mostly only Kelvin waves and no other wave modes were investigated. Also most analyses focus on zonal wavenumbers 1–2, neglecting the higher wavenumbers also important for the dynamics of the QBO.

This has been shown in an analysis by Tindall et al. (2006a,b) in the tropopause region using ERA-15 temperature and wind data: In particular higher zonal wavenumbers 4–7 also contribute significantly to the momentum flux of the waves. Since the momentum transfer of the different wave types is one of the key drivers of the dynamics of the QBO these high wavenumbers cannot be neglected.

A comprehensive study in the troposphere was made by Wheeler and Kiladis (1999) using OLR data. In a follow-up investigation a similar analysis was made by Cho et al. (2004) using TRMM rainfall data. These analyses cover the source processes of the waves observed at higher altitudes in the stratosphere.

In the stratosphere, different from the troposphere, in particular, the Kelvin waves (but also other equatorial wave types) observed in the stratosphere cover a larger range of

periods. Therefore, for example, the stratospheric Kelvin waves can be classified in ultraslow (periods 25–30 days, Canziani, 1999), slow (periods 10–20 days, Shiotani et al., 1997), fast (periods 6–10 days, Hitchman and Leovy, 1988), and ultrafast waves (periods 3–4 days, Salby et al., 1984; Lieberman and Riggin, 1997; Garcia et al., 2005). The

5　low-frequency waves will not propagate to higher altitudes because they will encounter critical level filtering and wave breaking. In this way the waves interact with the QBO and drive the wind reversal in the stratosphere. On the other hand very high-frequency (short-period) waves are able to penetrate the atmosphere up to the thermosphere. This is why we would expect that the higher up in the atmosphere the more important

10　are the waves with the higher phase speeds and the longer vertical wavelengths and higher equivalent depths (e.g., Salby et al., 2007; Takahashi et al., 2007).

Although a lot of detailed work about equatorial wave modes has been carried out in the stratosphere (see above) there is still some kind of lack of systematic climatological investigations of the different equatorial wave modes based on stratospheric satellite

15　data sets spanning several years.

SABER data have a large potential for the analysis of equatorial waves. A first analysis over a short time period of SABER data with focus on the mesosphere and lower thermosphere has already been carried out by Garcia et al. (2005). Now, having over 4 years of high-quality temperature data from the SABER instrument spanning from the

20　tropopause region to above 100 km with a good resolution of about 2 km vertically and covering zonal wavenumbers of up to about 6–7 (owing to the orbit parameters of the TIMED satellite) we have the opportunity to carry out a more comprehensive analysis also in the stratosphere.

2 Space-time spectral analysis method for equatorial wave modes in SABER and ECMWF data

2.1 Analysis method

To separate symmetric from antisymmetric wave modes often a spectral analysis is carried out dividing the spectral power into its symmetric and antisymmetric parts with respect to the equator (e.g., Wheeler and Kiladis, 1999).

Every data field $\Psi(\lambda, \Phi, t)$ can be written as sum of its symmetric $\Psi_{symm}(\lambda, \Phi, t)$ and its anti-symmetric $\Psi_{anti}(\lambda, \Phi, t)$ parts (λ: longitude, Φ: latitude, t: time):

$$\Psi(\lambda, \Phi, t) = \frac{1}{2}(\Psi(\lambda, \Phi, t) + \Psi(\lambda, -\Phi, t))$$
$$+ \frac{1}{2}(\Psi(\lambda, \Phi, t) - \Psi(\lambda, -\Phi, t))$$
$$=: \Psi_{symm}(\lambda, \Phi, t) + \Psi_{anti}(\lambda, \Phi, t) \tag{4}$$

And we also obtain symmetric $\hat{\Psi}_{symm}(k, \omega; \Phi)$ and anti-symmetric $\hat{\Psi}_{anti}(k, \omega; \Phi)$ spectral power after Fourier transform in longitude and time (k: zonal wavenumber, ω: wave frequency). The total spectral power contained in $\Psi(\lambda, \Phi, t)$ is:

$$\hat{\Psi}(k, \omega; \Phi) = \sum_{\lambda, t} \Psi(\lambda, \Phi, t) \exp(i(k\lambda + \omega t))$$
$$= \sum_{\lambda, t} \left(\Psi_{symm}(\lambda, \Phi, t) + \Psi_{anti}(\lambda, \Phi, t)\right)$$
$$\times \exp(i(k\lambda + \omega t))$$
$$= \hat{\Psi}_{symm}(k, \omega; \Phi) + \hat{\Psi}_{anti}(k, \omega; \Phi) \tag{5}$$

Since equatorial wave modes are expected to be either symmetric or antisymmetric with respect to the equator often the symmetric and antisymmetric spectral power are

treated independently and each averaged over a latitude band (e.g., 15 S–15 N) to increase the signal to noise ratio.

In our case the data analyzed in this way are residual temperatures from the SABER instrument and European Centre for Medium-Range Weather Forecasts (ECMWF) analyses. The ECMWF model is described, for example in Coy and Swinbank (1997).

We use a windowed Fourier analysis based on non-overlapping 31-day time windows. The choice of this window length is some kind of compromise between the expected temporal variations of the data and at the same time still a sufficient frequency resolution. For example, in the upper stratosphere effects due to the semi-annual oscillation (SAO) can be found, so the window length has to be well below 3 months not to smooth out the temporal variations. On the other hand ultraslow Kelvin waves can have periods of about 30 days which can still be resolved with the window length used. In addition, also the stationarity of the wave modes we expect to find plays an important role as we expect to find also shorter period waves than in the troposphere.

2.2 Analysis of SABER data

The SABER instrument onboard the TIMED satellite measures temperatures and several trace gases from the tropopause region to above 100 km (e.g., Mlynczak, 1997; Russell et al., 1999; Yee et al., 2003). In this paper we will analyze temperature residuals from the zonal mean for version 1.06 SABER temperature data.

With the TIMED orbit cycle of about 1.7 h (i.e., 14 orbits/day) SABER data can resolve zonal wavenumbers up to 6–7 and frequencies up to about 1 cycle/day. Further details about the asynoptic sampling geometry of low Earth orbiting satellites can be found in, e.g., Hayashi (1980); Salby (1982a,b); Wu et al. (1995). Due to the asynoptic sampling simple fast Fourier transform (FFT) cannot be applied to the satellite data. Instead, we use a least-squares method similar to the approach described by Wu et al. (1995) which has already been used by Smith et al. (2002) to estimate the space-time Fourier coefficients for an analysis of equatorial wave signatures in CRISTA temperature data. This kind of approach can also cope with data gaps as well as irregular

Equatorial wave analysis from SABER and ECMWF temperatures

M. Ern et al.

Equatorial wave analysis from SABER and ECMWF temperatures

M. Ern et al.

satellite sampling pattern (Wu et al., 1995), which is important because the TIMED satellite performs yaw maneuvers every 60 days due to solar angle restrictions.

We obtain residual SABER temperatures by subtracting the zonal wavenumber zero of a Kalman filter analysis, giving a temporally evolving estimate for the zonal mean on a daily basis. The data set we use ranges from February 2002 until March 2006. The equatorial wave analysis of SABER temperatures is carried out in 4° latitude bins centered at the equator and ±4, ±8, ±12, ... degrees latitude. The analysis covers altitudes in 1-km steps, starting at 20 km as the lowermost altitude to avoid altitudes with increased noise due to cloud-contamination of the observations. The uppermost analysis altitude was above 100 km, however, we will focus on the stratospheric analyses in the altitude range 20–50 km and a comparison to results from ECMWF in this paper.

Figures 2a and 2b show space-time spectra of symmetric and antisymmetric spectral power density at 21 km altitude, averaged over the whole period analyzed (Feb. 2002 until Mar. 2006) and over latitudes 14 S–14 N (i.e., the analyses for the latitude bins 0, ±4, ±8, ±12 degrees are averaged) from SABER residual temperatures. Also given are the lines for equivalent depths of 8 and 90 m as well as the "tropospheric" spectral ranges used for integration of the total spectral contributions of the different wave types in Sect. 3.

It first should be mentioned that in stratospheric temperatures we obviously do not have a red noise-like background spectrum dominating over most of the spectral signatures of equatorial waves like in Wheeler and Kiladis (1999) or Cho et al. (2004), who analyzed tropospheric OLR and precipitation data. In our analysis of stratospheric temperatures the spectral peaks of Kelvin waves in symmetric spectral power and of Rossby-gravity waves in antisymmetric power are the most prominent spectral features (beneath equatorial Rossby waves at very low frequencies and diurnal variations at ±1 cpd). This means the general spectral features due to equatorial wave modes observed by, e.g., Wheeler and Kiladis (1999) and Cho et al. (2004) in the troposphere are also present in the stratosphere.

Different from the tropospheric observations we find in the average spectra shown in

Fig. 2 also contributions of the different wave types outside the range of "tropospheric" equivalent depths. This indicates that waves excited by processes of very deep convection play an important role already in the lower stratosphere at 21 km altitude.

Beneath the abovementioned spectral peaks we find some kind of continuous spectral background which is about constant in the wavenumber/frequency-domain. For both symmetric and antisymmetric spectra it is about $0.15\,K^2$/wavenumber/cpd. By integrating over the whole wavenumber/frequency-domain in both symmetric and antisymmetric spectra, which have to be treated separately, this would be equal to a contribution of about $2\,K^2$ of SABER temperature variances (total contribution from symmetric and antisymmetric backgrounds added).

Of course, this background is composed of measurement noise, interpolation errors, spectral leakage and aliasing, contributions from inertia-gravity waves, but the main contribution are probably localized gravity waves which are not resolved by the analysis method, playing also an important role in equatorial atmospheric dynamics (see Sect. 1).

The contribution of inertia-gravity waves with $n>0$ cannot be extracted easily from this background. Therefore inertia-gravity waves with $n>0$ will not be subject of this paper.

2.3 Analysis of ECMWF data

The ECMWF data set we use has a spatial resolution of 1 deg longitude times 1 deg latitude. Data are available daily for 0, 6, 12, 18 GMT on 28 pressure levels between 1013.25 and 0.1 mbar. Because we are mainly interested in a comparison between SABER and ECMWF we use only ECMWF data from the same period where SABER data are available (Feb. 2002 until Mar. 2006) and focus on stratospheric altitudes.

The ECMWF data offer a much better space-time resolution than the SABER data. Zonal wavenumbers as high as 180 and frequencies up to 2 cycles/day can be resolved. For the current analysis such high resolution is not required. We use the full latitudinal resolution of 1 deg, but only a reduced data set with 9 deg longitude resolu-

tion. To make sure that the variance of the data is not affected we simply omit ECMWF grid points in our analysis. Full resolution control runs show that almost no information is lost because most equatorial wave activity is at zonal wavenumbers lower than 15.

Different from the SABER analysis residual temperatures are determined by remov-
⁵ ing the mean and the trend via linear fits determined for every time window, pressure level and latitude. But since the time windows used are relatively short (31 days) there are no contaminations by the annual cycle and the results of the analyses show that the method of detrending the data has almost no effect. Another difference to the SABER analysis is that, owing to the fact that ECMWF data are given on a regular grid in space
¹⁰ and time, the FFT can be used to determine the space-time Fourier coefficients.

2.4 Comparison of the SABER and ECMWF analyses

Like the average SABER spectra shown in Figs. 2a and 2b, Figs. 2c and 2d show space-time spectra of symmetric and antisymmetric spectral power density at 21 km altitude, averaged over the whole period analyzed (Feb. 2002 until Mar. 2006) and
¹⁵ over latitudes 15 S–15 N for ECMWF. Please note that also the color scales are the same as in Figs. 2a and 2b.

There are striking similarities in the shape of the spectral peaks of Kelvin, equatorial Rossby, and Rossby-gravity waves. Even the occurrence of fast Kelvin or Rossby-gravity waves outside the "tropospheric" spectral bands can be found in the ECMWF
²⁰ data. Again, it is difficult to separate the contribution of inertia-gravity waves from the background.

The most striking difference between average SABER and ECMWF spectra can be found in the quasi continuous background which is much lower in the ECMWF spectra. Partly this is an effect of the larger spectral region covered by ECMWF and the back-
²⁵ ground is spread over a much larger spectral area. Therefore a reduced background would be expected in Figs. 2c and 2d, which show only the part of the spectral domain common with the SABER analysis and not the full spectra. However, the total con-tribution of the ECMWF spectral background (symmetric and antisymmetric added) is

equivalent to temperature variance between about 0.5 and 0.7 K^2, which is considerably lower than the SABER value of about 2 K^2, indicating that this is not only an effect of the larger spectral domain covered by ECMWF. Smaller parts of this difference can be attributed to interpolation errors or measurement noise present in SABER data but not in ECMWF. The largest contribution, however, is most likely due to the broad spectrum of gravity waves which is present in SABER temperature data (e.g., Eckermann and Preusse, 1999; Preusse et al., 2002; Ern et al., 2004, 2005; Wu et al., 2006) but underrepresented in the ECMWF data used.

Figures 3a–3d show the average spectra for SABER and ECMWF at 41 km altitude. Compared to Figs. 2a and 2c the spectral peak attributed to Kelvin waves is shifted towards higher equivalent depths. For comparison the lines for equivalent depths 8, 90 and 2000 m are also shown. An equivalent depth of 2000 m corresponds to vertical wavelengths of about 50 km in the stratosphere.

This indicates that part of the Kelvin waves at low equivalent depths is absorbed in the lower stratosphere, thereby transferring momentum to the zonal wind system and driving the QBO. On the other hand Kelvin waves with higher equivalent depths, which have higher phase speeds, are not affected and can propagate towards higher altitudes. The effects observed for the other wave modes are similar.

The quasi continuous background in the SABER spectra is strongly enhanced compared to 21 km altitude. The temperature variances contributed to this background are about 7 K^2. This reflects the increase of the amplitudes of gravity waves with altitude. There is also an enhancement in the ECMWF background at 41 km altitude compared to 21 km. The temperature variance due to this background is about 3–4 K^2, again considerably lower than the SABER values. The contribution due to gravity waves will be discussed in more detail in Sect. 3.2.

The average peak Kelvin signal for the strongest wave components is given in Table 1 for both SABER and ECMWF at the altitudes 21, 32, and 41 km. We have chosen only the strongest spectral contributions because those should only be little influenced by differences in the spectral background (see also below). At altitudes below about

Equatorial wave analysis from SABER and ECMWF temperatures

M. Ern et al.

Title Page

Abstract	Introduction
Conclusions	References
Tables	Figures

|◄ | ►|

◄ | ►

Back | Close

Full Screen / Esc

Printer-friendly Version

Interactive Discussion

EGU

32 km the values given in Table 1 for SABER and ECMWF are very similar and mostly do not differ by more than 10–20%. At higher altitudes the peak spectral power densities from ECMWF are higher than the SABER values on average and can exceed the SABER values by 50% and more. This can also be seen from Fig. 4 where the average deviation of the 10 strongest 4-year average Kelvin wave components is plotted against the altitude (solid line). Also given in Fig. 4 is the relative deviation of the total ECMWF Kelvin wave variances from the SABER variances (long dashed line) in the spectral region $k=1$–6 and frequencies between 0.03 and 0.4 cycles/day. ECMWF variances are somewhat lower in the lower stratosphere and about the same in the upper stratosphere.

However, it should be noted that the deviations shown in Table 1 and Fig. 4 are emphasized since the power spectral densities given are normalized squared wave amplitudes. The relative deviations of the corresponding wave amplitudes are smaller by a factor of two.

This means that not only the relative distribution of the spectra is very similar, but also the absolute values are in good agreement in the lower stratosphere. In the upper stratosphere ECMWF tends to overestimate Kelvin wave components.

3 Timeseries for the different wave components

3.1 Equatorial wave modes

In the previous section average spectra at 21 km and 41 km altitude were shown and good agreement was found between SABER and ECMWF. Now the question arises whether this agreement still holds if we extend the comparison over the whole stratosphere and take into account the temporal evolution of equatorial wave activity.

In a first step we integrate the power spectral density over the spectral bands between 8 and 90 m equivalent depth which are attributed to the most prominent source processes in the troposphere. The "tropospheric" spectral bands used for integration

are indicated as white shaded areas in Figs. 2a–d.

Figure 5 shows the altitude-time cross-sections obtained for SABER and Fig. 6 for ECMWF. The values given are temperature variances calculated from the integrated power spectral densities. Shown are the contributions due to (a) Kelvin waves, (b) inertia-gravity waves (n=0), (c) equatorial Rossby waves (n=1), and (d) Rossby-gravity waves, respectively. The contributions due to inertia-gravity waves (n>0) and equatorial Rossby waves (n=2) are not shown because the amplitudes are rather small compared to the spectral background.

Overplotted in Figs. 5 and 6 are contour lines of the zonal mean zonal wind from ECMWF averaged over the 31-day windows used and all latitudes from 15 S–15 N. The contour interval is 10 m/s. Solid lines indicate eastward, dashed lines westward wind. The zero wind line is highlighted by a boldface solid line.

As expected there is an evident modulation of the temperature variances by the QBO below about 40 km altitude. Eastward propagating wave modes show enhanced values during QBO east phases (i.e., phases of westward directed zonal winds) while westward propagating wave modes are enhanced during QBO west phases (i.e., phases of eastward directed zonal winds). Above about 40 km altitude the semiannual variation (SAO) is dominating in the temperature variances.

Kelvin waves are the by far dominant wave mode in residual temperatures, reaching temperature variances of about $1 K^2$ during QBO east phases. Temperature variances of the other wave modes are small compared to the Kelvin waves.

Figures 7 and 8 show the same as Figs. 5 and 6, but for the contributions of higher equivalent depths outside the "tropospheric" band of 8–90 m equivalent depth. The variances shown were obtained by integrating the power spectral density between 90 and 2000 m equivalent depth. The upper value of 2000 m is chosen somewhat arbitrarily to cover all relevant spectral contributions in the altitude range considered we attribute to Kelvin waves. In the following we will call these wave bands "fast" wave bands. For comparison the lines for 2000 m are also shown in Figs. 3a–d. This choice, for example, would also include the ultrafast Kelvin waves identified by Salby et al.

(1984), having wavenumber 1 and periods of about 3.5 days.

Similar as in Wheeler and Kiladis (1999) we cut the spectral bands used for integration at 0.4 cpd for Kelvin waves and at 0.5 cpd for eastward inertia-gravity waves (n=0) and −0.5 cpd (i.e., periods longer than about 2 days) for Rossby-gravity waves to avoid too large overlaps with the frequency bands attributed to tides and inertia-gravity waves with higher values of n>0.

From Figs. 7a and 8a we can see that for the Kelvin waves obviously the modulation of the spectral power in the "fast" wave band is not as strong as for the "tropospheric" wave band, especially in the middle and upper stratosphere. For the Kelvin waves in the "tropospheric" wave band variances vary from about 0.1 K^2 to about 1 K^2 between maximum and minimum values in the stratosphere. This means there is a contrast of a factor of about 10 caused by QBO modulation. In the SABER "fast" wave band (Fig. 7a) the contrast between maximum and minimum variance, for example, is only a factor of about 2–3 at 30 km altitude.

It is also remarkable that the QBO induced maxima of the "tropospheric" wave band are very narrow and occur mainly during periods of eastward shear in the westward wind of the QBO east periods (see also Ratnam et al., 2006). This means that these waves are closely related with the downward phase propagation of the westward background winds of the QBO east phases. Different from this the "fast" band Kelvin waves display a broad maximum spread over the whole QBO east periods and are modulated much stronger by the SAO. There are even indications of modulations due to the SAO in the middle stratosphere. It should be noted that these fast band waves are not visible in the analyses by Tsai et al. (2004); Randel and Wu (2005) and Ratnam et al. (2006) using GPS data because their method is only able to resolve waves with periods longer than about 7–10 days.

There is a considerable contribution of the "fast" band waves already in the lower stratosphere, which can be of the same order as the contribution from the "tropospheric" band waves during the periods when the "tropospheric" band waves reach their maximum. During all other periods the "fast" band waves are dominant. In the

upper stratosphere and above the "fast" band waves are always dominant.

For the equatorial Rossby waves the "tropospheric" wave band shows a variation with the QBO whereas the variations of "fast" wave band variances are a mixture of QBO modulation and an annual cycle. For the Rossby-gravity waves the QBO variation is the main contribution in both wave bands, whereas the $n=0$ inertia-gravity waves show QBO variations in the "tropospheric" band and no clear signatures for the "fast" band waves. Maybe this is due to the fact that the "fast" band as we have defined it is very narrow in order to exclude contributions of higher n inertia-gravity waves.

Overall we can see that the equatorial wave activity in the stratosphere can be divided in two parts. One part at low equivalent depths is modulated mainly by the QBO winds, the other part at higher equivalent depths shows also annual variations or variations due to the SAO. This behavior is found in both SABER and ECMWF residual temperatures, again showing the surprising agreement between both data sets.

3.2 Contribution of gravity waves

We also calculate the temperature variances due to gravity waves by estimating the spectral background in both symmetric and antisymmetric spectra. To avoid contamination of this background value by the equatorial wave modes we omit the tidal peaks, as well as zonal wavenumbers lower than 3 (where the main contributions of equatorial waves are located) and calculate the median of the power spectral density from the remaining spectrum. This is done separately for both symmetric and antisymmetric spectra. By doing so the spectral peaks of the equatorial waves do not influence the result of the background value, which would be the case for an average value over the whole spectrum.

These symmetric and antisymmetric median background values are added to obtain the background value for the complete spectrum. Then this constant value is integrated over the full spectrum and divided by two (because the power spectral densities given are squared amplitudes and not variances) to obtain the temperature variance due to gravity waves.

The resulting altitude-time distribution is shown in Fig. 9 for SABER (Fig. 9a) and ECMWF (Fig. 9b). Over the whole altitude range the variances due to gravity waves in the SABER data obviously are considerably higher than in ECMWF (please note that the color scales in Figs. 9a and 9b are different). SABER gravity wave variances range from about $1.5–2\,K^2$ in the lower stratosphere to about $15–20\,K^2$ in the upper stratosphere, monotonically increasing.

The range of ECMWF gravity wave variances is from about $0.5–0.7\,K^2$ in the lower stratosphere to about $3–5\,K^2$ in the upper stratosphere, decreasing again above 44 km altitude.

The SABER gravity wave variances show an annual cycle in the lower stratosphere which is less pronounced in the equatorial waves (compare Figs. 5–8). In addition there are also variations due to the QBO with maximum variances at about the same times as the "tropospheric" wave band Kelvin waves. In the upper stratosphere the gravity waves show variations due to the SAO. ECMWF variances show similar variations, but less pronounced.

This behavior agrees with previous findings from SABER residual temperatures using a different method (Krebsbach and Preusse, 2006) and from GPS radio occultation measurements (Wu, 2006; de la Torre et al., 2006). For a more detailed discussion see Sect. 4.2

4 Comparison to previous analyses

4.1 Equatorial waves

As mentioned in Sects. 2.2–2.4 the general behavior of the spectral signatures we find in SABER and ECMWF temperatures in the stratosphere is similar to the characteristics observed in the troposphere (e.g., Wheeler and Kiladis, 1999; Cho et al., 2004). However we also find spectral contributions at higher equivalent depths/higher phase speeds. Higher phase speed Kelvin waves have been observed before by, e.g., Salby

et al. ([1984](#)); Hitchman and Leovy ([1988](#)); Lieberman and Riggin ([1997](#)); Garcia et al. ([2005](#)).

For a quantitative comparison, we compare our results to the analyses of GPS temperature data mentioned above (Tsai et al., [2004](#); Randel and Wu, [2005](#); Ratnam et al., [2006](#)). In these analyses Kelvin wave activity of zonal wavenumbers 1 and 2 with periods longer than about 7–10 days is covered (Ratnam et al., [2006](#)). These are the main contributions also present in the "tropospheric" wave bands of SABER and ECMWF data. Therefore temperature variances of the GPS analyses can directly be compared to our "tropospheric" Kelvin wave band variances.

The structures in the altitude/time cross-sections (Figs. [5](#) and [6](#)) are quite similar to the ones shown in Ratnam et al. ([2006](#)). Peak values of temperature amplitudes in the middle stratosphere observed by Ratnam et al. ([2006](#)) are about $1-1.5\,K^2$ as an average over the dominant wavenumber 1 and 2 components. This would result in temperature variances of about $1-2\,K^2$ if we assume that both wavenumber 1 and 2 have the same amplitudes. This is in good agreement with the peak values of about $1-1.5\,K^2$ for the "tropospheric" wave band in SABER and ECMWF data (see Figs. [5](#) and [6](#)).

These values are also in good agreement with findings from radiosonde observations. For example Angell et al. ([1973](#)) find peak variances of about $2\,K^2$ at the equator in their 12-year data set at 50 mbar for wave periods between 10 and 20 days. In another example by Sato et al. ([1994](#)) for wave periods between 8 and 20 days peak temperature variances between about 1 and $2.5\,K^2$ in the altitude region 20–30 km are found for a 15-year data set of routine rawinsondes at Singapur. These values are somewhat higher than the $0.5-1.5\,K^2$ in our "tropospheric" Kelvin wave band. This difference can easily be explained because the values of our analysis represent an average over the latitudes from about 15 S–15 N and equatorial wave activity decreases towards higher latitudes. In addition, our "tropospheric" Kelvin wave band not fully coincides with the waves resolved by the radiosonde analyses.

Equatorial wave analysis from SABER and ECMWF temperatures

M. Ern et al.

Title Page

Abstract	Introduction
Conclusions	References
Tables	Figures

◄◄ ►►

◄ ►

Back | Close

Full Screen / Esc

Printer-friendly Version

Interactive Discussion

EGU

4.2 Gravity waves

The variances of gravity waves shown in Fig. 9a are derived from space-time spectra of SABER residual temperatures. The values obtained can be compared to values derived by Preusse et al. (2006) using a different method based on a vertical harmonic analysis using altitude profiles of SABER residual temperatures. These residual temperatures were obtained by subtracting a background distribution estimated with a zonal wavenumber 0–6 Kalman filter.

For the equatorial region the values given in Fig. 2 of Preusse et al. (2006) for August 2003 are about 7 dB of temperature squared amplitudes at about 20 km altitude and about 14 dB at about 50 km altitude, corresponding to squared amplitudes of about $5\,K^2$ and $25\,K^2$, respectively, i.e., temperature variances of about $2.5\,K^2$ and $12.5\,K^2$, respectively.

The values we obtain from the space-time spectra for August 2003 are about $2\,K^2$ at 20 km altitude and about $10\,K^2$ for 50 km altitude (see Fig. 9a). This is a very good agreement, taking into account that the two methods for determining gravity wave temperature variances are very different.

The temporal evolution of variances due to wave activity in the equatorial region including gravity waves has been investigated before by, for example, Wu (2006) and de la Torre et al. (2006) using GPS radio occultation measurements. The observed pattern is very similar to the one observed for Kelvin waves. Since these analyses are based on vertical profiles of residual temperatures obtained by merely vertical detrending the results were a mixture between global equatorial wave modes (mainly Kelvin waves) and gravity waves.

In an analysis by Krebsbach and Preusse (2006) based on the SABER gravity wave squared amplitudes by Preusse et al. (2006) annual variations as well as QBO related variations were found in the lower stratosphere and variations due to the SAO were found in the upper stratosphere. This general behavior can also be seen in the results presented in Sect. 3.2, confirming the finding that also gravity waves are modulated by

Title Page

Abstract | Introduction

Conclusions | References

Tables | Figures

◄ | ►

◄ | ►

Back | Close

Full Screen / Esc

Printer-friendly Version

Interactive Discussion

EGU

the QBO. The amplitude of the QBO variation found by Krebsbach and Preusse (2006) is about 0.2 K in the stratosphere.

In Sect. 2.2 we have found an average temperature variance of about $2\,K^2$ due to gravity waves in the lower stratosphere (i.e., amplitudes of about 2 K). An estimate for maximum and minimum amplitudes due to the QBO modulation is then given by $2\,K\pm0.2\,K$ using the QBO amplitude of 0.2 K by Krebsbach and Preusse (2006). Therefore there should be a modulation of the temperature variances between $1.8^2\,K^2/2$ and $2.2^2\,K^2/2$ due to the QBO, i.e. between about $1.6\,K^2$ and $2.4\,K^2$ which is in good agreement with the values of about 1.8 and $3\,K^2$ which can be seen from Fig. 9a.

The amplitude of the annual cycle seen by Krebsbach and Preusse (2006) is between about 0.05 and about 0.2 K in the equatorial region between 15S and 15N. The distribution is not centered at the equator. An average amplitude that could be compared with our results would be about 0.1 K around 25 km altitude. Repeating the above estimation results in minimum and maximum variances of about 1.8 and $2.2\,K^2$ that would be expected according to Krebsbach and Preusse (2006). This means the annual variation should be less pronounced than the variation due to the QBO, and this is also what we find from Fig. 9a.

It should be noted that the above estimates for the QBO and annual variations of gravity wave variances are not more than some kind of cross-check. In addition the stronger annual cycle observed at the lowermost altitudes in SABER data is not seen in GPS measurements (e.g., de la Torre et al., 2006) and could be an indication that at the lowermost altitudes the SABER temperatures might be influenced by clouds.

5   Kelvin wave activity during the SCOUT-O3 tropical aircraft campaign

For field campaigns meteorological analyses like, for instance, the ECMWF analyses are of great importance for mission planning during measurement campaigns as well as for the analysis of the collected data. Therefore it is an important information how reliable, for example, the horizontal and temporal distribution of equatorial waves is

represented in the meteorological data.

One method often used to get an overview of the spatial and temporal variation are Hovmoeller plots, i.e., 2d plots of a meteorological parameter versus longitude and time.

Here we present the example of the Kelvin wave activity during the SCOUT-O3 tropical aircraft campaign in Darwin/Australia during November and December 2005. Again, we average over the latitudes 15 S–15 N, but we use 91-day analysis windows to avoid minor inconsistencies which would occur at the transition between adjacent analysis windows.

Figure 10a shows a Hovmoeller plot of undetrended ECMWF temperatures at 21 km altitude, averaged over the latitudes 15 S–15 N in the period from 27 October until 27 December, 2005. It should be noted that by averaging the temperatures over a latitude band symmetric with respect to the equator antisymmetric equatorial waves cancel out and we can compare the resulting average temperature distribution only with symmetric equatorial wave analyses.

Apart from some smaller scale fluctuations due to the diurnal cycle and small scale processes the main feature in Fig. 10a apparently is a mixture of eastward propagating waves. The eastward propagation direction can be seen from the phase fronts which are tilted from the upper left towards the lower right. This information together with the fact that Kelvin waves are the most dominant process in tropical temperatures we can infer that these temperature structures are caused by a mixture of Kelvin waves.

This assumption can be confirmed by Figs. 10b and 10c. These two figures show the residual temperatures obtained by inverting the power spectra of the equatorial wave analysis filtered for the combined "tropospheric" and "fast" Kelvin wave band between 8 and 2000 m equivalent depth. Figures 10b and 10c show the residual temperatures obtained from ECMWF and SABER, respectively.

Again, we find good agreement between the SABER and the ECMWF spectral analyses. Deviations between Figs. 10b and 10c are less than about 1.5 K maximum and about 0.3 K on average. At the same time the difference between maximum and min-

imum values in Figs. 10b and 10c is about 6 K and the average deviation from zero is about 0.7 K for both data sets if unsigned absolute values are taken. This means that in the lower stratosphere ECMWF analyses do not only agree very well with the SABER temperature variances, they are also able to reproduce the temporal evolution of zonal temperature structures very well.

The Kelvin waves observed have pronounced periods of about 10–15 days, and, indeed, there is a mixture of Kelvin waves, leading to the observed residual temperatures of about ±3 K maximum. The fact that we have a mixture of Kelvin waves, and not a single monochromatic one, is the reason why residual temperatures are maximum at longitudes 50E–180E, i.e., in the Darwin region, where the measurement campaign took place.

If we compare Figs. 10b and 10c with Fig. 10a we can see that most of the temperature variations symmetric with respect to the equator can be explained by Kelvin waves. (Please note that there is a temperature cooling trend in Fig. 10a masking some of the relative structures.) From Figs. 5–8 we can see that strong variations due to Kelvin waves could be expected because the SCOUT-O3 campaign in Darwin took place during a QBO east period with enhanced Kelvin wave activity in the lower stratosphere.

6 Conclusions

We carried out an analysis for equatorial waves based on four-year (Feb. 2002 until Mar. 2006) data sets of SABER and ECMWF temperatures. We divided the equatorial waves into symmetric and antisymmetric wave modes, similar to the analysis by Wheeler and Kiladis (1999). This method performed well for both the asynoptic data set of SABER satellite measurements as well as the ECMWF meteorological analyses, given on a regular grid. Both data sets are obviously capable to resolve longer period waves as well as short period waves, at least down to periods of about 2 days.

The spectral signatures of Kelvin waves, equatorial Rossby waves, inertia-gravity

waves (n=0), as well as Rossby-gravity waves can be identified clearly throughout the stratospheric altitude range of 20–50 km considered in this paper. We find that the equatorial wave activity in a slow phase speed wave band between 8 and 90 m equivalent depth, which is normally attributed to the convective processes in the troposphere acting as source of the equatorial waves, is mainly modulated by the QBO.

Different from this the waves at higher equivalent depths (90–2000 m) show less pronounced variation due to the QBO. Also effects of SAO and annual cycle can be found. For Kelvin waves the contribution of these "fast" waves cannot be neglected even in the lower stratosphere.

We find good agreement between our analyses and previous studies based on satellite data (e.g., analysis of GPS temperatures by Ratnam et al., 2006) as well as analyses based on radiosonde measurements (e.g., Angell et al., 1973). It is also remarkable that there is very good agreement between the SABER and ECMWF analyses. Only in the upper stratosphere ECMWF tends to overestimate Kelvin wave components (in some cases by more than 50%). There is agreement not only in the spectra, but also in the temporal evolution of the temperature variances and even in the longitudinal distribution of residual temperatures and their temporal evolution in the lower stratosphere, which has been demonstrated at an altitude of 21 km for the case of the SCOUT-O3 campaign in Darwin/Australia, November/December 2005.

From our space-time analysis we are also able to derive the temperature variances of gravity waves from the spectral background for both SABER and ECMWF space-time spectra. The results for SABER are in good agreement with previous results by Preusse et al. (2006) and Krebsbach and Preusse (2006) while ECMWF underestimates the variances due to gravity waves by a factor of about 3.

This shows on one hand that the SABER data are an excellent data set providing high-resolution data with large spatial coverage and on the other hand that although ECMWF tends to overestimate Kelvin wave components at higher altitudes and small scale fluctuations are underrepresented the ECMWF data are also able to reliably reproduce measurements of equatorial waves at least in the lower stratosphere, making

Equatorial wave analysis from SABER and ECMWF temperatures

M. Ern et al.

ECMWF a valuable tool accompanying measurement campaigns.

References

Alexander, M. J., Holton, J. R., and Durran, D. R.: The gravity wave response above deep convection in a squall line simulation, J. Atmos. Sci., 52, 2212–2226, 1995. 11688

Angell, J. K., Cotton, G. F., and Korshover, J.: A climatological analysis of oscillations of Kelvin wave period at 50 mb, J. Atmos. Sci., 30, 13–24, 1973. 11689, 11702, 11707

Baldwin, M. P., Gray, L. J., Dunkerton, T. J., Hamilton, K., Haynes, P. H., Randel, W. J., Holton, J. R., Alexander, M. J., Hirota, I., Horinouchi, T., Jones, D. B. A., Kinnersley, J. S., Marquardt, C., Sato, K., and Takahashi, M.: The quasi-biennial oscillation, Rev. Geophys., 39, 179–229, 2001. 11686, 11687

Bergman, J. W. and Salby, M. L.: Equatorial wave activity derived from fluctuations in observed convection, J. Atmos. Sci., 51, 3791–3806, 1994. 11689

Canziani, P. O., Holton, J. R., Fishbein, E., Froidevaux, L., and Waters, J. W.: Equatorial Kelvin waves: A UARS MLS view, J. Atmos. Sci., 51, 3053–3076, 1994. 11689

Canziani, P. O.: Slow and ultraslow equatorial Kelvin waves: The UARS CLAES view, Q. J. R. Meteorol. Soc., 125, 657–676, doi:10.1256/smsqj.55413, 1999. 11690

Chang, C.-P.: Vertical structures of tropical waves maintained by internally-induced cumulus heating, J. Atmos. Sci., 33, 729–739, 1976. 11688, 11689

Cho, H.–K., Bowman, K. P., and North, G. R.: Equatorial waves including the Madden–Julian Oscillation in TRMM rainfall and OLR data, J. Climate, 17, 4387–4406, 2004 11689, 11693, 11701

Coy, L. and Swinbank, R.: Characteristics of stratospheric winds and temperatures produced by data assimilation, J. Geophys. Res., 102, 25 763–25 781, 1997. 11692

de la Torre, A., Schmidt, T., and Wickert, J.: A global analysis of wave potential energy in the lower stratosphere derived from 5 years of GPS radio occultation data with CHAMP, Geophys. Res. Lett., 33, L24809, doi:10.1029/2006GL027696, 2006. 11701, 11703, 11704

Equatorial wave analysis from SABER and ECMWF temperatures

M. Ern et al.

Title Page

Abstract	Introduction
Conclusions	References
Tables	Figures

|◀ | ▶|

◀ | ▶

Back | Close

Full Screen / Esc

Printer-friendly Version

Interactive Discussion

EGU

Dunkerton, T. J.: The role of gravity waves in the quasi-biennial oscillation, J. Geophys. Res., 102, 26 053–26 076, 1997. 11686

Eckermann, S. D., and Preusse, P.: Global measurements of stratospheric mountain waves from space, Science, 286, 1534–1537, 1999. 11696

Ern, M., Preusse, P., Alexander, M. J., and Warner, C. D.: Absolute values of gravity wave momentum flux derived from satellite data, J. Geophys. Res., 109, D20103, doi:10.1029/2004JD004752, 2004. 11696

Ern, M., Preusse, P., and Warner, C. D.: A comparison between CRISTA satellite data and Warner and McIntyre gravity wave parameterization scheme: Horizontal and vertical wavelength filtering of gravity wave momentum flux, Adv. Space Res., 35, 2017–2023, doi:10.1016/j.asr.2005.04.109, 2005. 11696

Fulton, S. R. and Schubert, W. H.: Vertical normal mode transforms: Theory and application, Mon. Wea. Rev., 113, 647–658, 1985. 11688, 11689

Garcia, R. R., Lieberman, R., Russell III, J. M., and Mlynczak, M. G.: Large-scale waves in the mesosphere and lower thermosphere observed by SABER, J. Atmos. Sci., 62, 4384–4399, 2005. 11690, 11702

Hayashi, Y.: A method of estimating space-time spectra from polar-orbiting satellite data, J. Atmos. Sci., 37, 1385–1392, 1980. 11692

Hitchman, M. H. and Leovy, C. B.: Estimation of the Kelvin wave contribution to the semiannual oscillation, J. Atmos. Sci., 45, 1462–1475, 1988. 11686, 11690, 11702

Johnson, R. H. and Ciesielski, P. E.: Rainfall and radiative heating rates from TOGA COARE atmospheric budgets, J. Atmos. Sci., 57, 1497–1514, 2000. 11689

Krebsbach, M. and Preusse, P.: Spectral analysis of gravity wave activity in SABER temperature data, Geophys. Res. Lett., 34, L03814, doi:10.1029/2006GL028040, 2006. 11701, 11703, 11704, 11707

Lieberman, R. S. and Riggin, D.: High resolution Doppler imager observations of Kelvin waves in the equatorial mesosphere and lower thermosphere, J. Geophys. Res., 102, 26 117–26 130, 1997. 11690, 11702

Lindzen, R. S.: The interaction of waves and convection in the tropics, J. Atmos. Sci., 60, 3009–3020, 2003. 11686, 11688

Matsuno, T.: Quasi-geostrophic motions in the equatorial area, J. Meteorol. Soc. Jpn., 44, 25–43, 1966. 11687

Mlynczak, M. G.: Energetics of the mesosphere and lower thermosphere and the SABER

Title Page

Abstract	Introduction
Conclusions	References
Tables	Figures

|◄ | ►|

◄ | ►

Back | Close

Full Screen / Esc

Printer-friendly Version

Interactive Discussion

EGU

instrument, Adv. Space Res., 44, 1177–1183, 1997. 11692

Pires, P., Redelsperger, J.-L., and Lafore, J.-P.: Equatorial atmospheric waves and their association to convection, Mon. Wea. Rev., 125, 1167–1184, 1997. 11686

Preusse, P., Dörnbrack, A., Eckermann, S. D., Riese, M., Schaeler, B., Bacmeister, J. T., Broutman, D., and Grossmann, K. U.: Space based measurements of stratospheric mountain waves by CRISTA, 1. Sensitivity, analysis method and a case study, J. Geophys. Res., 107, 8178, doi:10.1029/2001JD000699, 2002. 11696

Preusse, P., Ern, M., Eckermann, S. D., Warner, C. D., Picard, R. H., Knieling, P., Krebsbach, M., Russell III, J. M., Mlynczak, M. G., Mertens, C. J., and Riese, M.: Tropopause to mesopause gravity waves in August: Measurement and modeling, J. Atmos. Sol.–Terr. Phys., 68, 1730–1751. 11703, 11707

Randel, W. J., Boville, B. A., and Gille, J. C.: Observations of planetary mixed Rossby-gravity waves in the upper stratosphere, J. Atmos. Sci., 47, 3092–3099, 1990. 11689

Randel, W. J. and Gille, J. C.: Kelvin wave activity in the upper stratosphere observed in SBUV ozone data, J. Atmos. Sci., 48, 2336–2349, 1991. 11689

Randel, W. J. and Wu, F.: Kelvin wave variability near the equatorial tropopause observed in GPS radio occultation measurements, J. Geophys. Res., 110, D03102, doi:10.1029/2004JD005006, 2005. 11686, 11689, 11699, 11702

Ratnam, M. V., Tsuda, T., Kozu, T., and Mori, S.: Long-term behavior of the Kelvin waves revealed by CHAMP/GPS RO measurements and their effects on the tropopause structure, Ann. Geophys., 24, 1355–1366, 2006,
http://www.ann-geophys.net/24/1355/2006/. 11689, 11699, 11702, 11707

Russell III, J. M., Mlynczak, M. G., Gordley, L. L., Tansock, J., and Esplin, R.: An overview of the SABER experiment and preliminary calibration results, Proceedings of SPIE, 3756, 277–288, 1999. 11692

Salby, M. L.: Sampling theory for asynoptic satellite observations, Part I: Space-time spectra, resolution, and aliasing, J. Atmos. Sci., 39, 2577–2600, 1982. 11692

Salby, M. L.: Sampling theory for asynoptic satellite observations, Part II: Fast Fourier synoptic mapping, J. Atmos. Sci., 39, 2601–2614, 1982. 11692

Salby, M. L., Hartmann, D. L., Bailey, P. L., and Gille, J. C.: Evidence for equatorial Kelvin modes in Nimbus–7 LIMS, J. Atmos. Sci., 41, 220–235, 1984. 11689, 11690, 11698, 11701

Salby, M. L., and Garcia, R. R.: Transient response to localized episodic heating in the tropics, Part I: Excitation and short-time near-field behavior, J. Atmos. Sci., 44, 458–498, 1987.

Title Page

Abstract | Introduction

Conclusions | References

Tables | Figures

◄◄ | ►►

◄ | ►

Back | Close

Full Screen / Esc

Printer-friendly Version

Interactive Discussion

EGU

11688

Salby, M. L., Matrosova, L., and Callaghan, P. F.: Global Kelvin waves in the upper atmosphere excited by tropospheric forcing at midlatitudes, J. Geophys. Res., 112, D06111, doi:10.1029/2006JD007235, 2007. 11690

Sato, K., Hasegawa, F., and Hirota, I.: Short-period disturbances in the equatorial lower stratosphere, J. Meteorol. Soc. Jpn., 72, 859–873, 1994. 11689, 11702

Semeniuk, K., and Shepherd, T. G.: Mechanisms for tropical upwelling in the stratosphere, J. Atmos. Sci., 58, 3097–3115, 2001. 11687

Shiotani, M., Gille, J. C., and Roche, A. E.: Kelvin waves in the equatorial lower stratosphere as revealed by cryogenic limb etalon spectrometer temperature data, J. Geophys. Res., 102(D22), 26 131–26 140, 1997. 11690

Shuckburgh, E., Norton, W., Iwi, A., and Haynes, P.: Influence of the quasi-biennial oscillation on isentropic transport and mixing in the tropics and subtropics, J. Geophys. Res., 106(D13), 14 327–14 337, 2001. 11687

Smith, A. K., Preusse, P., and Oberheide, J.: Middle atmosphere Kelvin waves observed in Cryogenic Infrared Spectrometers and Telescopes for the Atmosphere (CRISTA) 1 and 2 temperature and trace species, J. Geophys. Res., 107(D23), 8177, doi:10.1029/2001JD000577, 2002. 11692

Srikanth, R. and Ortland, D. A.: Analysis of Kelvin waves in High-Resolution Doppler Imager and Microwave Limb Sounder stratosphere measurements using a constrained least squares method, J. Geophys. Res., 103(D18), 23 131–23 151, 1998. 11689

Straub, K. H. and Kiladis, G. N.: The observed structure of convectively coupled Kelvin waves: Comparison with simple models of coupled wave instability, J. Atmos. Sci., 60, 1655–1668, 2003. 11686

Takahashi, H., Wrasse, C. M., Fechine, J., Pancheva, D., Abdu, M. A., Batista, I. S., Lima, L. M., Batista, P. P., Clemesha, B. R., Schuch, N. J., Shiokawa, K., Gobbi, D., Mlynczak, M. G., and Russell, J. M.: Signature of ultra fast Kelvin waves in the equatorial middle atmosphere and ionosphere, Geophys. Res. Lett., 34, L11108, doi:10.1029/2007GL029612, 2007. 11690

Tindall, J. C., Thuburn, J., and Highwood, E. J.: Equatorial waves in the lower stratosphere. I: A novel detection method, Q. J. R. Meteorol. Soc., 132, 177–194, doi:10.1256/qj.04.152, 2006. 11688, 11689

Tindall, J. C., Thuburn, J., and Highwood, E. J.: Equatorial waves in the lower stratosphere. II: Annual and interannual variability, Q. J. R. Meteorol. Soc., 132, 195–212,

doi:10.1256/qj.04.153, 2006. 11689

Tsai, H.-F., Tsuda, T., Hajj, G. A., Wickert, J., and Aoyama, Y.: Equatorial Kelvin waves observed with GPS occultation measurements (CHAMP and SAC-C), J. Meteorol. Soc. Jpn., 82, 397–406, 2004. 11689, 11699, 11702

5 Wallace, M. W. and Kousky, V. E.: Observational evidence of Kelvin waves in the tropical stratosphere, J. Atmos. Sci., 25, 900–907, 1968. 11689

Wheeler, M. and Kiladis, G. N.: Convectively coupled equatorial waves: Analysis of clouds and temperature in the wavenumber-frequency domain, J. Atmos. Sci., 56, 374–399, 1999. 11688, 11689, 11691, 11693, 11699, 11701, 11706

10 Wu, D. L., Hays, P. B., and Skinner, W. R.: A least squares method for spectral analysis of space–time series, J. Atmos. Sci., 52, 3501–3511, 1995. 11692, 11693

Wu, D. L., Preusse, P., Eckermann, S. D., Jiang, J. H., Juarez, M. D. L. T., Coy, L., and Wang, D. Y.: Remote sounding of atmospheric gravity waves with satellite limb and nadir techniques, Adv. Space Res., 37, 2269–2277, 2006. 11696

15 Wu, D. L.: Small-scale fluctuations and scintillations in high-resolution GPS/CHAMP SNR and phase data, J. Atmos. Sol.–Terr. Phys., 68, 999–1017, 2006. 11701, 11703

Wu, Z., Sarachik, E. S., and Battisti, D. S.: Vertical structure of convective heating and the three-dimensional structure of the forced circulation on an equatorial beta plane, J. Atmos. Sci., 57, 2169–2187, 2000. 11688

20 Yanai, M. and Maruyama, T.: Stratospheric wave disturbances propagating over the equatorial Pacific, J. Meteorol. Soc. Jpn., 44, 291–294, 1966. 11689

Yee, J. H., Talaat, E. R., Christensen, A. B., Killeen, T. L., Russell, J. M., and Woods, T. N.: TIMED instruments, Johns Hopkins APL Technical Digest, 24, 156–164, 2003. 11692

Equatorial wave analysis from SABER and ECMWF temperatures

M. Ern et al.

Title Page

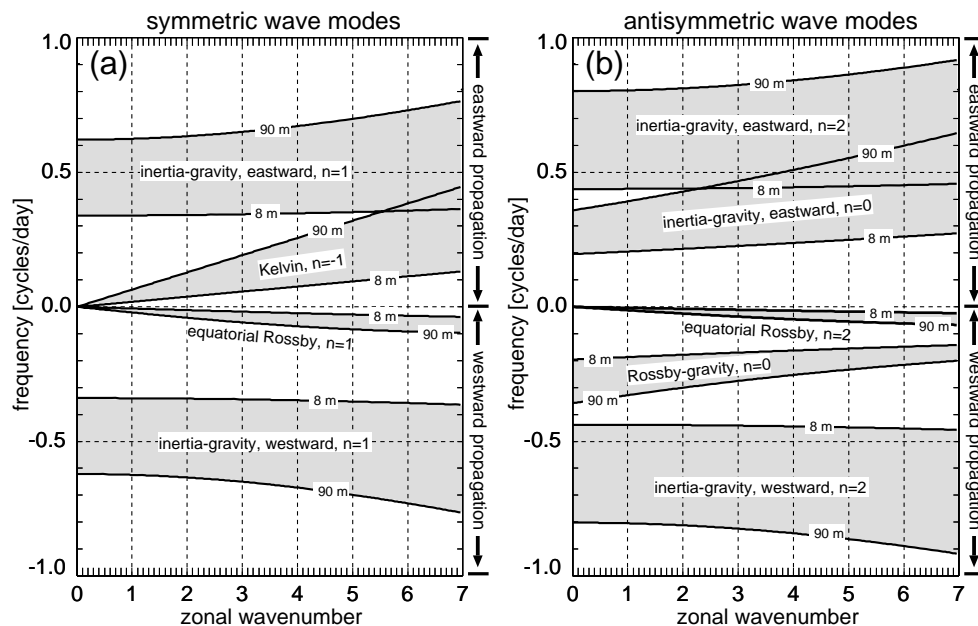| Abstract | Introduction |
| Conclusions | References |
| Tables | Figures |

|◄ | ►|

◄ | ►

Back | Close

Full Screen / Esc

Printer-friendly Version

Interactive Discussion

EGU

Table 1. Power spectral density of the strongest Kelvin wave components in the four-year average SABER and ECMWF temperature analyses at 21, 32, and 41 km altitude.

k: zonal waveno., T: period [days]	SABER power spectral density [K^2/waveno/cpd]	ECMWF power spectral density [K^2/waveno/cpd]
altitude: 21 km		
k=1, T=15.50	6.32	6.11
k=1, T=10.33	6.62	6.42
k=2, T=10.33	3.52	3.72
k=2, T= 7.75	2.98	2.62
k=2, T= 6.20	2.14	1.74
altitude: 32 km		
k=1, T=15.50	5.13	6.47
k=1, T=10.33	8.50	11.27
k=1, T= 7.75	4.55	4.37
k=1, T= 6.20	2.50	2.37
k=2, T= 7.75	3.37	3.95
k=2, T= 6.20	3.29	3.89
k=2, T= 5.17	2.27	2.58
altitude: 41 km		
k=1, T=15.50	4.57	9.21
k=1, T=10.33	9.20	18.14
k=1, T= 7.75	8.13	12.02
k=1, T= 6.20	6.92	8.74
k=2, T= 7.75	2.41	4.75
k=2, T= 6.20	4.82	6.12
k=2, T= 5.17	4.24	5.73
k=2, T= 4.43	3.01	4.13

EGU

Fig. 1. Spectral ranges between equivalent depth $h_e=8$ m and $h_e=90$ m for the most relevant equatorial wave modes in the horizontal wavenumber/frequency domain.
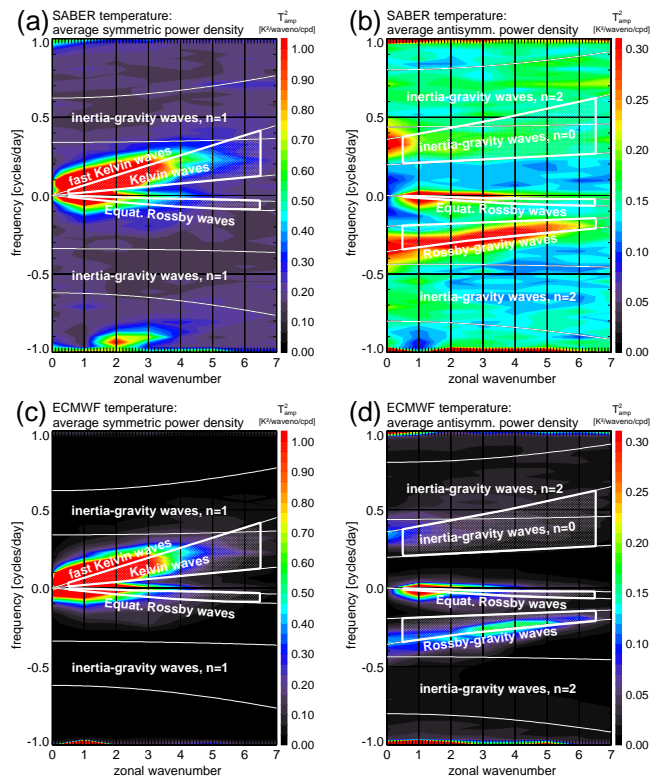
Fig. 2. Space-time spectra of SABER temperature symmetric **(a)** and antisymmetric **(b)** power density at 21 km altitude, averaged over the whole period analyzed (Feb. 2002 until Mar. 2006) and over latitudes 14 S–14 N (i.e., the analyses for the latitude bins 0, ±4, ±8, ±12 degrees are averaged). Also shown: ECMWF temperature symmetric **(c)** and antisymmetric **(d)** power density at 21 km altitude, averaged over the whole period analyzed (Feb. 2002 until Mar. 2006) and over latitudes 15 S–15 N. For comparison the lines for equivalent depths of 8, and 90 m are given for the different wave modes, as well as the "tropospheric" wave bands used for integrating the spectral power in Sect. 3.

EGU
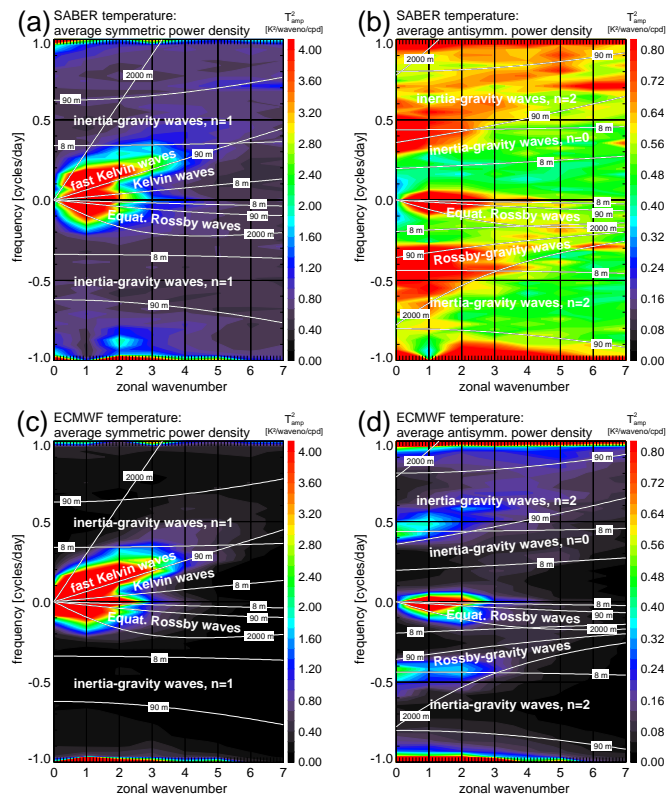
Fig. 3. Space-time spectra of SABER temperature symmetric **(a)** and antisymmetric **(b)** power density at 41 km altitude, averaged over the whole period analyzed (Feb. 2002 until Mar. 2006) and over latitudes 14 S–14 N (i.e., the analyses for the latitude bins 0, ±4, ±8, ±12 degrees are averaged). Also shown: ECMWF temperature symmetric **(c)** and antisymmetric **(d)** power density at 41 km altitude, averaged over the whole period analyzed (Feb. 2002 until Mar. 2006) and over latitudes 15 S–15 N. For comparison the lines for equivalent depths of 8, 90, and 2000 m are given for the different wave modes.
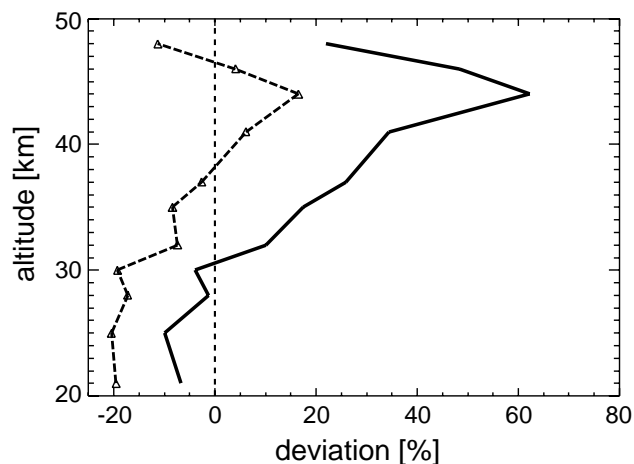
Fig. 4. Altitude profile of the average deviation between the corresponding ECMWF analysis components and the 10 strongest 4-year average Kelvin wave components in the SABER analysis (bold solid line). Also given: the relative deviation of the total ECMWF Kelvin wave variances from the SABER variances (long dashed line).
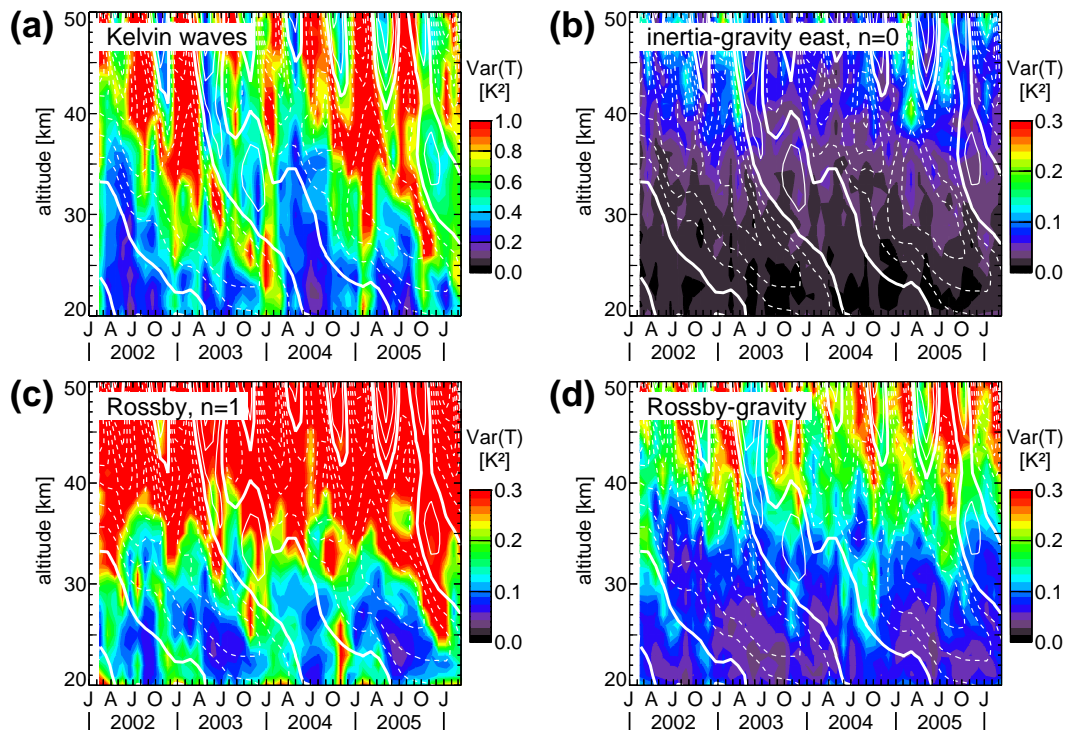
Fig. 5. Altitude-time cross-sections of SABER temperature variances integrated over the "tropospheric" wave bands between 8 and 90 m equivalent depth for **(a)** Kelvin waves, **(b)** inertia-gravity waves (n=0), **(c)** equatorial Rossby waves (n=1), and **(d)** Rossby-gravity waves. Overplotted contour lines are zonal mean zonal wind from ECMWF averaged over the latitudes 15 S–15 N. Contour interval is 10 m/s, solid lines indicate eastward, dashed lines westward wind. The zero wind line is highlighted by a boldface solid line.

Fig. 6. Altitude-time cross-sections of ECMWF temperature variances integrated over the "tropospheric" wave bands between 8 and 90 m equivalent depth for **(a)** Kelvin waves, **(b)** inertia-gravity waves (n=0), **(c)** equatorial Rossby waves (n=1), and **(d)** Rossby-gravity waves. Overplotted contour lines are zonal mean zonal wind from ECMWF averaged over the latitudes 15 S–15 N. Contour interval is 10 m/s, solid lines indicate eastward, dashed lines westward wind. The zero wind line is highlighted by a boldface solid line.

Title Page

Abstract | Introduction

Conclusions | References

Tables | Figures

◄◄ | ►►

◄ | ►

Back | Close

Full Screen / Esc

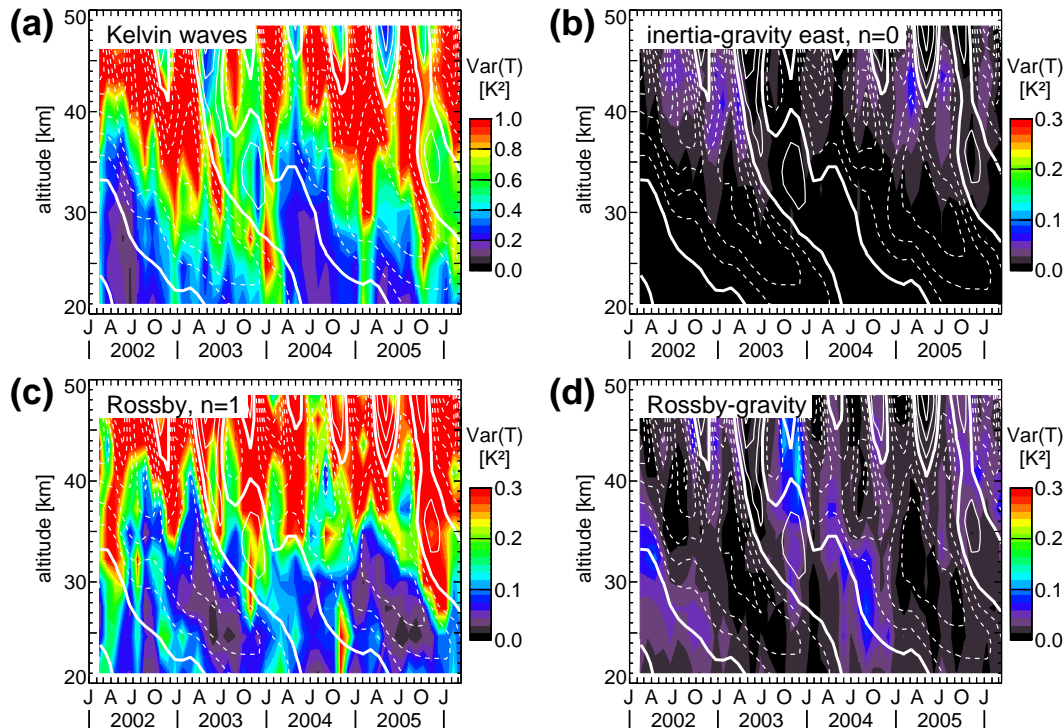Printer-friendly Version
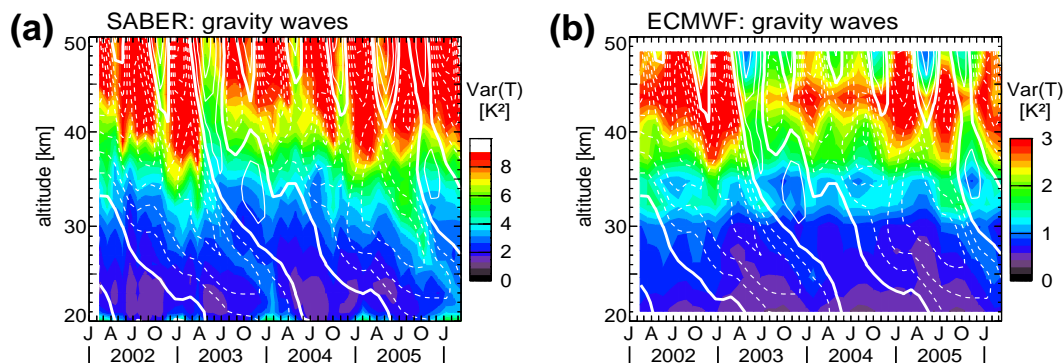
Interactive Discussion

EGU

Fig. 7. Altitude-time cross-sections of SABER temperature variances integrated over the "fast" wave bands between 90 and 2000 m equivalent depth for **(a)** Kelvin waves, **(b)** inertia-gravity waves (n=0), **(c)** equatorial Rossby waves (n=1), and **(d)** Rossby-gravity waves. Overplotted contour lines are zonal mean zonal wind from ECMWF averaged over the latitudes 15 S–15 N. Contour interval is 10 m/s, solid lines indicate eastward, dashed lines westward wind. The zero wind line is highlighted by a boldface solid line.

ACPD

7, 11685–11723, 2007

Equatorial wave analysis from SABER and ECMWF temperatures

M. Ern et al.

Title Page

Abstract | Introduction

Conclusions | References

Tables | Figures

|◄ | ►|

◄ | ►

Back | Close

Full Screen / Esc

Printer-friendly Version

Interactive Discussion

EGU

Fig. 8. Altitude-time cross-sections of ECMWF temperature variances integrated over the "fast" wave bands between 90 and 2000 m equivalent depth for **(a)** Kelvin waves, **(b)** inertia-gravity waves (n=0), **(c)** equatorial Rossby waves (n=1), and **(d)** Rossby-gravity waves. Overplotted contour lines are zonal mean zonal wind from ECMWF averaged over the latitudes 15 S–15 N. Contour interval is 10 m/s, solid lines indicate eastward, dashed lines westward wind. The zero wind line is highlighted by a boldface solid line.

EGU

Fig. 9. Altitude-time cross-sections of SABER **(a)** and ECMWF **(b)** temperature variances due to gravity waves. The variances were determined from the spectral background in the space-time spectra. Please note that the color scales in (a) and (b) differ by a factor of 3. Overplotted contour lines are zonal mean zonal wind from ECMWF averaged over the latitudes 15 S–15 N. Contour interval is 10 m/s, solid lines indicate eastward, dashed lines westward wind. The zero wind line is highlighted by a boldface solid line.
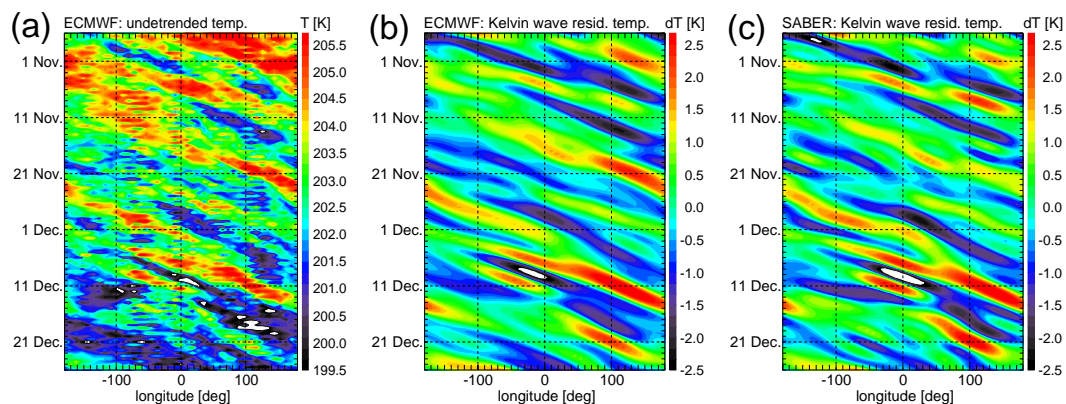
Fig. 10. Hovmoeller diagrams at 21 km altitude for the period of the SCOUT-O3 tropical aircraft measurement campaign from 27 October until 27 December 2005. **(a)** undetrended ECMWF temperatures averaged over the latitudes 15 S–15 N, **(b)** ECMWF residual temperatures derived from the space-time spectral analysis for the Kelvin wave band between 8 and 2000 m equivalent depth ("tropospheric" plus "fast" wave bands), and **(c)** SABER residual temperatures derived from the space-time spectral analysis for the same Kelvin wave band as in (b).

Title Page

Abstract   Introduction

Conclusions   References

Tables   Figures

◄◄   ►►

◄   ►

Back   Close

Full Screen / Esc

Printer-friendly Version

Interactive Discussion

EGU